

# An advanced signal processing technique for deriving grain size information of bedload transport from impact plate vibration measurements

Julien Barrière,<sup>1,3\*</sup> Andreas Krein,<sup>2</sup> Adrien Oth<sup>3</sup> and Reimar Schenkluhn<sup>4</sup>

<sup>1</sup> National Museum of Natural History (Mnhn), Walferdange, Grand Duchy of Luxembourg

<sup>2</sup> Public Research Centre – Gabriel Lippmann, Department of Environment and Agro-Biotechnologies, Belvaux, Grand Duchy of Luxembourg

<sup>3</sup> European Centre for Geodynamics and Seismology, Walferdange, Grand Duchy of Luxembourg

<sup>4</sup> Faculty VI Regional and Environmental Sciences, University of Trier, Trier, Germany

Received 30 May 2014; Revised 18 November 2014; Accepted 9 December 2014

\*Correspondence to: Julien Barrière, National Museum of Natural History (Mnhn), 19, Rue Josy Welter, L-7256 Walferdange, Grand Duchy of Luxembourg.

E-mail: julien.barriere@ecgs.lu

---

# ESPL

Earth Surface Processes and Landforms

**ABSTRACT:** A reliable characterization of bedload transport is required to gauge the engineering and theoretical issues related to the dynamics of sediments transport in rivers. However, while significant advances have been made in the development of monitoring techniques, robust quantitative predictive relationships have proven difficult to derive. In this article, we develop a dedicated signal processing technique aimed at improving the usage of impact plate measurements for material transport characterization. Our set-up consists of a piezoelectric hydrophone mounted on the bottom side of a stainless steel plate, thus acting as a ‘sediment vibration sensor’. While the classical analysis with such systems is usually limited to rather simple procedures, such as impact counting, a large amount of useful information is contained in the actual waveform of the impact signal, which conveys the force and the contact time that the bedload imposes on the plate. An advanced signal processing technique called ‘first arrival atomic decomposition’ is used to improve the characterization of bedload transport by analysing the amplitude and frequency attributes of each single impact. This new processing approach proves to be well suited for bedload transport monitoring using plate systems and allows us to establish a relationship between the median grain size ( $D_{50}$ ) and the impact signal properties. This link is first observed and validated with controlled flume experiments and then applied to continuous impact records in a small gravel-bed river during a flood event. The estimated  $D_{50}$  offers a novel possibility to observe the time-varying grain size distribution of bedload transport. Copyright © 2014 John Wiley & Sons, Ltd.

**KEYWORDS:** bedload transport; impact plate sensor; chirplet atomic decomposition; flume experiment; Hertz’s contact theory

## Introduction

A significant fraction of the mass transported by running water consists of bedload resulting from channel disturbances (e.g. erosion, flooding, sedimentation) that may affect the stability of entire river networks, from mountain systems to low-altitude streams (Lord *et al.*, 2009). Material accumulation can, for instance, cause damages to weirs, barrages or sluices (Ergenzinger and Schmidt, 1993; Badoux *et al.*, 2014). Traditional bedload measuring devices such as sediment samplers have been successfully used for many decades to investigate mass transport kinetics (Reid *et al.*, 1980; Laronne and Reid, 1993; Habersack and Laronne, 2001). However, the collection of sampled bedload data is often too expensive and laborious for practical purposes, encouraging researchers to look for relations estimating bedload transport rates (Gomez, 2006). Yet most of these empirical relations provide unsatisfactory results in gravel-bed rivers (Gray *et al.*, 2010) as well as in mountain rivers (Yager

*et al.*, 2007). In an attempt to overcome these limitations, new monitoring techniques based on the analysis of the acoustic fingerprint of bedload motion using passive or active sensors have been recently developed (see Gray *et al.*, 2010, for a complete review). Robust scaling relationships connecting acoustic measurement parameters to bedload transport rates would be of high interest in terms of monitoring capabilities, since these would in principal allow for a quantitative characterization of bedload transport in near-real time.

In the last decade, vibration measurements performed with plate or pipe geophone/hydrophone systems have been of growing interest for coarse materials (>2 mm) transport monitoring (Hegg and Rickenmann, 1998; Mizuyama *et al.*, 2010; Rickenmann *et al.*, 2012). Recent developments on different devices and methods for monitoring bedload movement (e.g. horizontal pipe system, impact plate sensors for different scales or river cross sections) are described in Gray *et al.* (2010). These investigations mainly focused on the recording of impulses produced by the

moving bedload, and the overall conclusions are that (1) gravel material can be detected and (2) the beginning and end of bedload movement can be determined acoustically. Bogen *et al.* (2003) and Rickenmann *et al.* (2013) present similar results from a range of case studies in catchments around the world.

Belleudy *et al.* (2010) and Barton *et al.* (2010) introduce passive monitoring approaches, where a hydrophone is placed near the riverbed to record the acoustic wave field resulting from water flow and bedload transport. Promising results were achieved regarding the detection of coarse sediments motion (>8 mm), but the technique proved to be highly sensitive to contamination by surrounding noise sources, rendering it unsuitable when the impact energies are too small. In another recent paper, Turowski and Rickenmann (2011) analyse the relationships between bedload transport rates, water discharge, and impact plate sensor response. They conclude that impact measurements alone are in most cases unsuitable to develop a rating curve for bedload transport rates. Nevertheless, relevant sensors such as the Swiss plate geophone can be used to estimate bedload volumes of individual events; the majority of these experiments focused on torrent channels in mountain environments (Rickenmann and McArdell, 2007; Turowski *et al.*, 2011; Rickenmann *et al.*, 2012, 2014). The same research team concludes that the results from these impact studies are in agreement with bedload volumes estimated from the survey of material stored in corresponding retention basins or captured with bedload basket traps (Rickenmann *et al.*, 2014). More recently, Turowski *et al.* (2013) made a first attempt to evaluate the energy delivered to the streambed by moving bedload using the same plate system, and Burtin *et al.* (2014) used similar impact measurements to constrain the potential contribution of bedload transport in the Illgraben catchment (Switzerland) to the seismic energy recorded with seismometers located nearby.

In contrast to these highly energetic cases, we aim to answer the question whether the use of impact plate measurements in streams in low mountain ranges (several hundred metres high) with comparatively low discharge and little bedload can also improve the characterization of material transport. The present study consists in the assessment of a new processing methodology of impact measurements using a hydrophone-based plate system, with experiments performed in two laboratory flumes and one field site near Trier (Germany). This type of set-up was first developed by Krein *et al.* (2008) and used to detect and characterize bedload movement in laboratory flume experiments. Since this article is devoted to the development and validation of a novel processing approach through controlled laboratory experiments, we provide an extensive description of the impact signal processing and the results acquired with the flume experiments. A well-defined relationship is found between the median grain size ( $D_{50}$ ) and impact signal attributes (frequency, amplitude) in agreement with the Hertz contact theory. Since this relation remains valid as long as the plate set-up and the grain size range (granular to pebble gravels) are unchanged, we show that the different impact signatures in a gravel-bed stream during a flood event are well explained by significant temporal changes of  $D_{50}$  according to laboratory observations.

## Experimental Set-up

### Impact plate system using a piezoelectric hydrophone

The impact plate system consists of a piezoelectric hydrophone mounted on the bottom side of a stainless steel plate (50 cm × 50 cm × 3 mm), detecting each single impact on the plate. The

hydrophone and plate are acoustically isolated from the subjacent fixing by rubber vibration cushions. The hydrophone is designed in such a way that it only records the mechanical friction on the surface of the metal plate below which it is fixed by screws. The advantage of this setup is that acoustic noise resulting from the water turbulence in the river is efficiently excluded. The ITC-4001 hydrophone is a shallow water transducer containing a flexural disc transducer. Its recording range lies between 0.1 and 20 kHz with a stable frequency response. This sensor is thus able to record acoustic signals in the sonic frequency range (kilohertz) with high signal-to-noise ratio (Krein *et al.*, 2008). The impact-generated vibrations in the plate are recorded with a portable data recorder (Zoom H4N wave-recorder), converted into digital signal with 16-bit resolution (.wav format) with absolute values varying between zero and one, high sampling rate (96 kHz), and stored on 32 GB SD-Cards.

### Laboratory flume experiments

Two laboratory flumes were used in this study. The first one is a small plexi-glass flume located at University of Trier, Germany, with a length of 3 m and a width of 0.27 m. In addition, it is tilt-able from 0° to 14° (Figure 1a). Although its size is not specifically dedicated to gravel transport experiments, such an apparatus can be useful to observe and record the various impact types that should occur in real conditions. A tank below the flume acts as a reservoir for the water circuit and sediment trap. An adjusted hydrophone plate is mounted at the end of the flume. The plate was downsized to half its original width to fit into the flume, which could in principle lead to a reduction of the variability of impact locations on the plate. The length of the plate is however preserved, thus still allowing for impacts to occur roughly up to the maximum distance from the sensor location, similar to the field set-up. We assume that this downsizing does not significantly affect the recorded vibration signal because the bending stiffness of the plate, fixed at its edges, should not be strongly modified in the Trier experiment. The influence of pump noise, which causes vibrations along the flume, was dampened by fixing silicon to the edges of the plate.

The laboratory set-up described here is, of course, a significant simplification of the expected situation in the field and, for this reason, a second, more realistic flume experiment was carried out at the University of Trondheim, Norway (Figure 1b). This experiment uses a significantly larger flume, with a length of 12.5 m and a width of 1 m, allowing for the same installation of the impact plate system as in the field (50 cm × 50 cm × 3 mm). For technical reasons, the slope was set to a fixed position (2°), and an efficient pumping system generated discharge levels up to 80 l s<sup>-1</sup> for the considered experiments. The main difference with the previous flume is that it allows for realistic transport of bedload sediments on an armoured bed ( $D_{16} = 1.15$  mm,  $D_{84} = 28$  mm) constituted by sand and gravels (Figure 1b, b1). Material moving over the steel plate is trapped in a basket, then weighed and sieved for comparison with the impact data.

### Field experiment

Impact measurements were also performed at a field site with the same apparatus as the one installed in the Trondheim experiment. In order to ensure highest possible consistency between the laboratory and the field experiments, the bedload material used in the flume experiment in Trier originates from this field site, and the sediments in the Trondheim experiment have similar density and shape. The shapes of the stones are randomly round, flat or angular, implying that this study is not

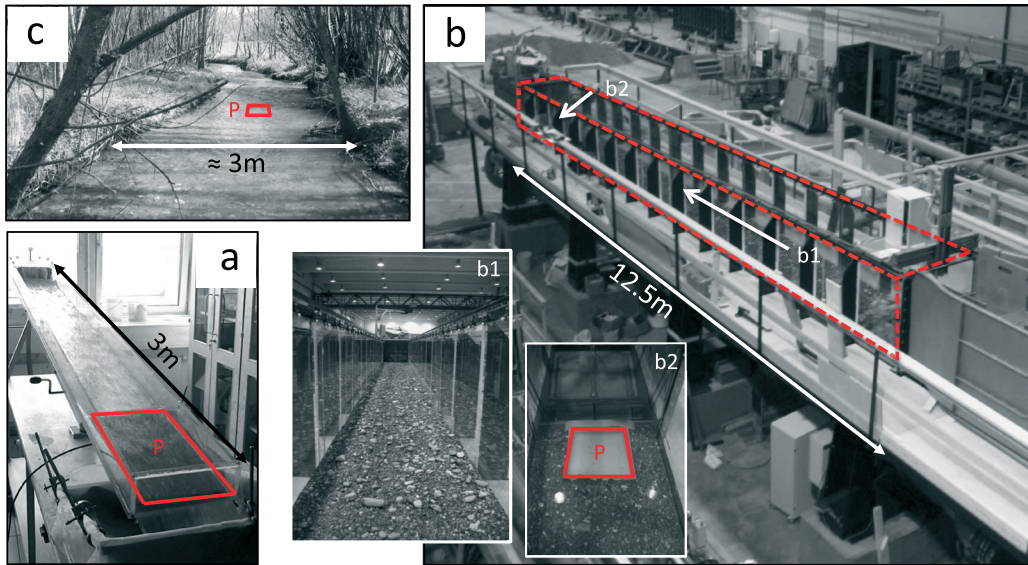


**Figure 1.** Pictures of (a) the Trier flume, (b) the Trondheim flume (dashed line) and (c) the Olewiger stream. Letter P corresponds to the impact plate. This figure is available in colour online at [wileyonlinelibrary.com/journal/espl](http://wileyonlinelibrary.com/journal/espl)

restricted to a certain range of shapes. The field site is located in a small gravel-bed river of the low-mountain range (Olewiger brook, Trier, Germany). The river cross-section is rectangular and its width reaches around 3 m in the considered portion (Figure 1c). The water level varies from one to a few dozen centimetres, depending on the flow intensity (discharge lower than  $5 \text{ m}^3 \text{ s}^{-1}$  during peak flow conditions). The mean channel slope is about 1.5% with a typical riffle pool sequence. Devonian shales with quartz and diabase veins dominate the geology, and the corresponding surface riverbed material is characterised by a  $D_{50}$  of  $8.7 \pm 3.9 \text{ mm}$  and a  $D_{90}$  of  $32.9 \pm 9.6 \text{ mm}$ . Detailed information about streambed morphology and sediment characteristics is given by Krein and Schorer (2000) or Peticrew *et al.* (2007). The contact plate with the hydrophone has been installed in the riverbed such that its upper surface is level with the sediment surface. The hydrophone is located in a cavity below the plate and thus not in contact with the riverbed. Start and stop trigger signals are controlled by a level sensor with magnetic float reacting to the water level. The recording procedure is started and continued as long as the pre-defined threshold level is constantly exceeded.

## Impact Signal Processing

### Analogy of impact measurements with the Hertz contact theory

In view of the high signal-to-noise ratio of the recorded impact signals, we aim to improve the classical ‘impact counting’ processing procedure (Rickenmann *et al.*, 2014) in order to derive more information on time-varying bedload properties. According to the Hertz contact theory and acoustic emission method literature (Tsunoda *et al.*, 1986; Buttle and Scruby, 1990; Uher and Benes, 2012), grain size can be estimated from acoustic measurements. Hertz’s theory allows for the calculation of the force time history that a round ball imposes on an elastic plate after being dropped at normal incidence (Johnson, 1985). The interaction of natural gravel particles with the metal plate, including different types of motion (saltation, rolling, sliding) and shapes (round, flat), is of course much more complex than in the case of a vertically impacting sphere. As noted by Krein *et al.* (2008), who used a similar apparatus, the shape of the

grains is decisive for the motion of the stones and thus also for the interaction with the contact plate. Stones with equally long axes (i.e. compact ones) have the lowest variability in their motions and produced similar signal patterns. In contrast, flat stones offer variable options to the attacking forces and may pass over the contact plate in very different modes, generating changing acoustic waveform (i.e. amplitude, frequency).

Nonetheless, a certain analogy with Hertzian contact might still be envisaged since the force pulse is highly dependent on the sphere size and mass. The impact signal generated by coarse or fine sediments, corresponding to the propagation of the flexural wave mode in the plate, should, therefore, have different statistical signatures despite the high variability of grain shapes, impact angles and velocity.

When a sediment particle impacts on the plate, the amplitude and frequency of the first arrival waveform are the two fundamental properties related to the force that the bedload imposes on the plate and the contact time defined as the duration over which the applied impact force is non-zero (Johnson, 1985). The amplitude and frequency of the raw data are directly interpretable as long as the measurement frequency lies in the linear frequency response range of the sensor and amplitude linearity over the entire full-scale range is ensured. Concerning the frequency attribute, we can associate the impact frequency to the mean frequency  $f_{\text{mean}}$  instead of the dominant frequency to take into account the overall shape of the impact frequency spectrum:

$$f_{\text{mean}} = \sqrt{\frac{\int_{-\infty}^{+\infty} |U(f)|^2 f^2 df}{\int_{-\infty}^{+\infty} |U(f)|^2 df}},$$

where  $U(f)$  is the Fourier spectrum and  $f$  the frequency.

If material properties are disregarded (i.e. assuming identical bulk properties among stones), the following proportionality relations may be assumed:

$$\begin{cases} f_{\text{mean}} \propto R^{-\alpha_1} \cdot V^{\beta_1} \\ A_{\text{max}} \propto R^{\alpha_2} \cdot V^{\beta_2} \end{cases}$$

where  $R$  is the mean radius of the particle,  $V$  the impact velocity,  $A_{\text{max}}$  the maximum signal magnitude (i.e. absolute value of amplitude), and  $\alpha_1$ ,  $\beta_1$ ,  $\alpha_2$  and  $\beta_2$  are real exponents. In some

acoustic emission studies (Uher and Benes, 2012; Pecorari, 2013), the values of these exponents have been estimated since experimental conditions were designed to fit the rather restrictive constraints under which Hertz contact theory can be considered as a rigorous theoretical framework. However, this theory is of course a strong simplification (e.g. elastic contact, infinite plate, normal incidence, round ball) regarding real-life impact-plate field measurements and our experimental conditions (e.g. varying shapes, motions and impact velocity/angle, uncertainty about the impact location on the plate). Therefore, we emphasize at this point that in this study, this simple model is not considered as a rigorous theoretical framework used to derive an exact formulation of the impact force, the time of contact, and consequently the frequency and amplitude attributes. Nevertheless, we can reasonably assume that at a given impact velocity, coarser and finer sediments will generate low frequency–high amplitude and high frequency–low amplitude waveforms, respectively. For both attributes, a shift towards higher frequencies and amplitudes should occur with increasing impact velocity. For the sake of notation simplicity,  $A_{\max}$  and  $f_{\text{mean}}$  are now referred to the variables  $A$  and  $F$ , respectively. As stated earlier, the aim of the following parts is not the development of an exact theoretical and mathematical framework, but the study represents an empirical and statistics-based approach in order to quantify bedload grain size from the statistical distribution of -amplitude/frequency attribute pairs from impact measurements.

### Time–frequency analysis of single stone dropping test

We performed a simple stone-dropping test to validate our choice for studying the relationship between amplitude–frequency ( $A$ – $F$ ) attributes and grain size. The possible drift due to changing impact velocity has not been taken into account here because its effect will be considered with the flume experiments presented in the Results and Discussion sections. For a drop height nearly constant (3–4 cm), we study the impact of two different grains on the steel plate at three different locations: 20 cm, 10 cm and 0 cm from the sensor located at the centre of the plate. The sediments used are a large and a small round gravel grain of 90 and 6 g, respectively. A time–frequency analysis is performed to examine the spectral properties of the different impact signals.

In the framework of time–frequency analysis, the Short Time Fourier Transform (STFT) is the logical continuation of Fourier analysis for non-stationary signals. The STFT is obtained through calculation of the Fourier transform of successive windowed portions of the signal, resulting in a two-dimensional time–frequency representation, often-called spectrogram (Oppenheim *et al.*, 1999). The continuous wavelet transform (CWT), which was introduced in the field of seismic processing (Goupillaud *et al.*, 1984), has a more flexible time–frequency resolution than the STFT and overcomes some of its limitations resulting from the fixed windowing function. The CWT is the integral over time of the signal  $x(t)$  multiplied by scaled and shifted versions of a function  $\psi$  called the mother wavelet (Mallat, 1999). The CWT results in wavelet coefficients  $C(a, b)$  depending on a scale,  $a$  and a translation factor,  $b$

$$C(a, b) = \frac{1}{\sqrt{a}} \int_{-\infty}^{+\infty} x(t) \bar{\psi}\left(\frac{t-b}{a}\right) dt,$$

where  $\bar{\psi}$  is the complex conjugate of the analysing wavelet function. The position  $b$  is generally associated with the

sampling interval  $\Delta$ . These wavelet coefficients constitute a time-scale map (scalogram) that can be converted into a time–frequency representation  $C(t, f_a)$  by assigning a pseudo-frequency  $f_a$  to the scale  $a$  using the relationship  $f_a = f_c/(a \cdot \Delta)$ , where  $f_c$  is the central frequency of the mother wavelet. As the mother wavelet, we use the complex Morlet wavelet, which is widely used in geophysics (Torrence and Compo, 1998):

$$\psi(t) = \frac{1}{\pi^{1/4}} \left( e^{i\omega_0 t} - e^{-\omega_0^2/2} \right) e^{-t^2/2},$$

where  $\omega_0 (=2\pi f_0)$  is the central angular frequency of the mother wavelet. The Morlet wavelet is a complex sinusoid confined within a Gaussian envelope  $e^{-t^2/2}$ . In order to satisfy some mathematical criteria to be considered as a wavelet, the second term in brackets corrects the complex Morlet wavelet for non-zero mean and becomes negligible for values of central frequency,  $\omega_0$ , higher than the standard limit value,  $\pi\sqrt{2/\ln 2}$  (Addison, 2002). If  $\omega_0$  decreases, the time resolution increases whereas the frequency resolution decreases. An increase in spectral resolution can be achieved by increasing  $\omega_0$  but the time localization will be unsuitable for time picking (i.e. the transform will be more spectral than temporal). In the following, the CWT will be computed using the standard value  $\omega_0 = \pi\sqrt{2/\ln 2}$  because it offers the best compromise between frequency and time resolution.

Figure 2 represents the signals recorded for the different impacts and the corresponding CWT time–frequency representation. First, the amplitude analysis in the time domain (Figures 2a and 2e for small and large grains, respectively) leads to the conclusion that the amplitude varies a lot with the impact location, but the magnitude for the bigger grain is significantly higher (twice or more). Therefore, the amplitude appears to be a valuable criterion, although insufficient on its own, to differentiate large from small grains. Time–frequency magnitude maps of these signals are depicted in Figures 2b–2d and 2f–2h for the small grain and the big grain cases, respectively. In the vicinity of the first arrival, the 90 g grain has a lower frequency signature than the 6 g sediment for all offsets. Nevertheless, the detection of the first arrival is difficult for large distances (10 and 20 cm) because the first event is of low amplitude and mixed with later arrivals resulting from rebounds of the grain on the plate and wave propagation effects in the plate, particularly from boundary reflections. This bad detection in the time–frequency plane is partly due to the chosen mother wavelet. Indeed, some other wavelets, such as the ‘Mexican hat’ wavelet (also called Ricker) or Morlet wavelet with lower  $\omega_0$  values, have fewer oscillations than the standard Morlet wavelet, allowing for a better temporal localization of singular short waveforms (Addison, 2002). However, a high number of vanishing moments (i.e. oscillations) constituting the analysing wavelet function are needed to obtain a meaningful CWT magnitude spectrum, comparable to the Fourier spectrum (Perrier *et al.*, 1995). In the family of signal decomposition techniques including STFT and CWT, dictionary-based methods (Mallat and Zhang, 1993) are better able to deal with complex waveforms such as the ones observed here for the overall impact signal, and are, therefore, expected to be more suitable to retrieve the  $A$ – $F$  information of the first arrival waveform. In the following part, we describe our dedicated processing algorithm called ‘first arrival atomic decomposition’ (FAAD), which was developed with a dictionary of chirplet functions (Bardainne *et al.*, 2006).

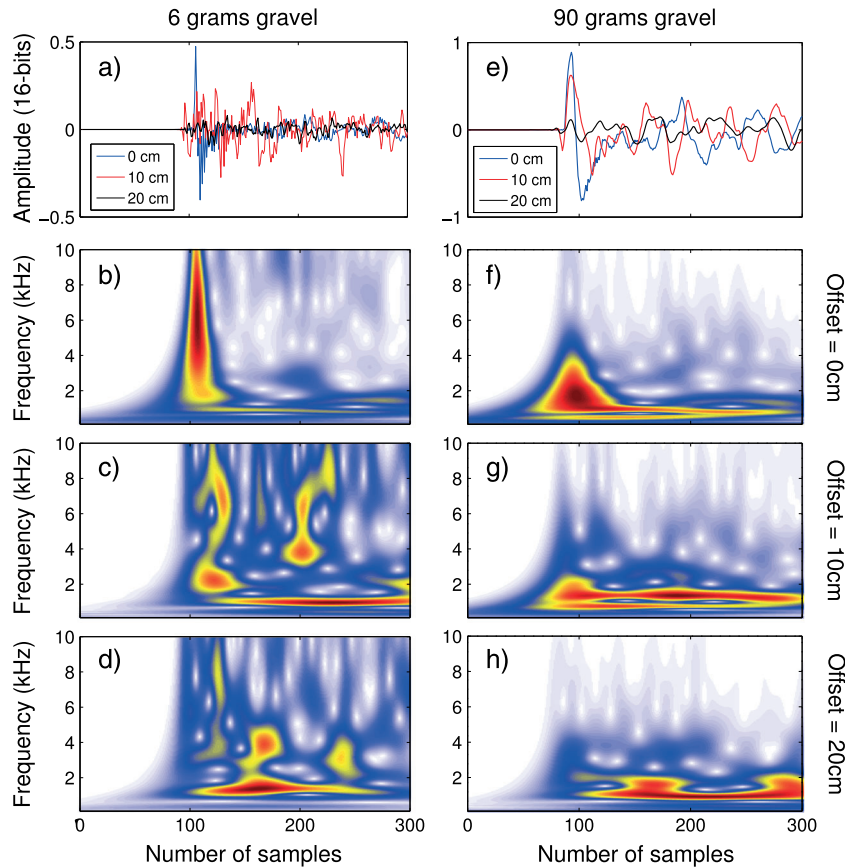


**Figure 2.** Recorded signal of 96 kHz sampling rate and its corresponding time–frequency transform (CWT using a standard Morlet wavelet) after dropping from a constant height (a) a 6 g gravel at (b) 0 cm, (c) 10 cm, (d) 20 cm from the sensor location and (e) a 90 g gravel at (f) 0 cm, (g) 10 cm, (h) 20 cm from the sensor location. The colour scale corresponds to the normalized magnitude of wavelet coefficients, red being the highest and blue-white the lowest values. Note the difficulty to detect a clear first arrival at large distance from the sensor. (See online version for the references to colour in this figure). This figure is available in colour online at [wileyonlinelibrary.com/journal/espl](http://wileyonlinelibrary.com/journal/espl)

### The first arrival atomic decomposition (FAAD)

Adaptive signal decomposition techniques represent a highly flexible tool to isolate events from mixed waves, and the

first arrival in one single iteration (i.e. one atom), and more elaborated atoms are needed. The chirplet developed by Mann and Haykin (1995) is well suited to our case and defined by:

$$C_k(a_k, t_k, f_k, q_k)(t) = |a_k| - \frac{1}{2}g\left(\frac{t_k - t}{a_k}\right) \exp\left[i\left(2\pi f_k(t_k - t) + \frac{q_k}{2}(t_k - t)^2\right)\right].$$

matching pursuit algorithm is commonly used in this field (Mallat and Zhang, 1993). This algorithm searches for the maximum correlation between the signal to be analysed and a dictionary of elementary functions called atoms. Once the best atom is found, it is extracted from the original signal and a residual is obtained. This procedure is repeated on the residual signal until a stopping criterion is reached (often related to the maximum signal energy to be recovered). It is then possible to rebuild the original signal as the sum of selected atoms weighted by real or complex coefficients. The processing that we developed is an adaptation of this algorithm since we want to perform one iteration only, in order to find one atom describing the first arrival as accurately as possible.

The choice of the atoms family constituting the dictionary is of primary importance. For instance, many wavelet functions such as those used for the CWT could be combined in the same dictionary. However, these two-dimensional functions are insufficient to correctly describe the complex

The chirp atom  $C_k$  is constructed from the Gaussian function  $g$  and described by four parameters: its central frequency,  $f_k$  and scale,  $a_k$  ( $f_k$  and  $a_k$  are independent, in contrast to the wavelet formulation), time,  $t_k$  and chirp rate,  $q_k$ . This last attribute describing the modulation in frequency is essential since we can expect to observe some dispersive behaviours for the wave mode propagating in the plate. This modulation is, however, considered to be linear and the definition of this four-dimensional chirplet might thus not always be optimal. In the context of seismology and induced-seismicity studies, Bardainne *et al.* (2006) have, therefore, proposed a generalization of the chirp atom to higher dimensions. By adding a non-linear modulation and two additional parameters modifying the symmetric Gaussian envelope, they were able to describe the overall complexity of noisy seismic signals. We choose this high dimensional atom dictionary for our processing because the structure of our recorded signals is very similar to typical signals present in seismic measurements. Since the formulation of this seven-dimensional chirplet function is complex and

beyond the scope of this paper, we refer the interested reader to the article of Bardainne *et al.* (2006) for a complete description.

Enlarging the atoms dictionary to seven dimensions is not straightforward and affects the computation time. We use the optimization procedures proposed by Gribonval (2001) and Bardainne *et al.* (2006) to speed up the computation. This optimization mainly rests on the hierarchical finding of the best chirp atom by searching for the maximum correlation in the Gabor atoms dictionary (sub-dictionary of the chirplet dictionary) described by only three free parameters, namely time, frequency and scale (see aforementioned references for more details). Finally, the FAAD algorithm provides an optimal reconstruction of the selected waveform in terms of chirp atom characterized by seven parameters that are a generalization of two-dimensional information obtained by wavelet transform in the time–frequency domain. To summarize, this complete processing technique, developed in the MATLAB environment, consists in two main steps illustrated in Figure 3:

- First arrival picking of each coherent impact in the time domain using a detection method similar to the STA/LTA (short-term average to long-term average) technique in seismology (e.g. Coppens, 1985; Earle and Shearer, 1994), which permits differentiating a signal onset within a noisy time history. The time corresponding to a high value of the STA/LTA ratio is considered to be a detection when the STA/LTA exceeds a user-defined threshold.
- Full characterization of the first waveform based on the chirplet atomic decomposition to get an accurate estimation of the  $A$ – $F$  attributes.

The first detection step is an important task that affects the reliability of the second one. Indeed, the efficiency of our algorithm depends strongly on its capacity to detect low as well as high amplitude impacts in the same record. Therefore, each record is analysed successively through five STA/LTA amplitude ranges, from the lowest to the highest threshold. Once one impact is detected in a given amplitude range, the corresponding

signal portion is removed from the scanning procedure for the other amplitude ranges to avoid a possible redundancy of detected impacts.

We set a maximum number of 60 impacts per minute and per amplitude range with a minimum spacing between impacts equal to one-tenth of a second. These setting parameters were identically chosen for laboratory and field measurements to ensure a reliable comparison between them. Enlarging these two limit criteria increases the computation time and potentially causes false first arrivals detections. The computation time is not really critical for the laboratory experiments because the analysed time intervals are typically only several minutes long, ranging from around 30 seconds for the shortest experiment (Trier) to 20 minutes for the longest one (Trondheim). However, for a natural flood event spreading over several hours or days, considering a maximum of 300 impacts per minute for the overall amplitude range is an acceptable limit to retrieve a well-defined acoustic signature. The processing of the whole flood event presented in this study required an important computational effort since the ratio between the computation time and the length of the entire record (almost 22 hours) is around three. A better ratio, lower than one, was achieved by parallelizing the code. Using a multi-core processor, the simplest way is to break up a long record into several shorter time series and analyse each part simultaneously by assigning one calculation (i.e. one part) to one single processor core.

## Results

### ‘Single grain class’ experiments

The first laboratory experiment was performed in the Trier flume with sieved and separated grain classes. The goal of these measurements is to obtain a reference  $A$ – $F$  signature for each selected grain class. After preliminary tests, we conclude that sediments below 2 mm are not satisfactorily detected because they generate a random high frequency noise of low amplitude

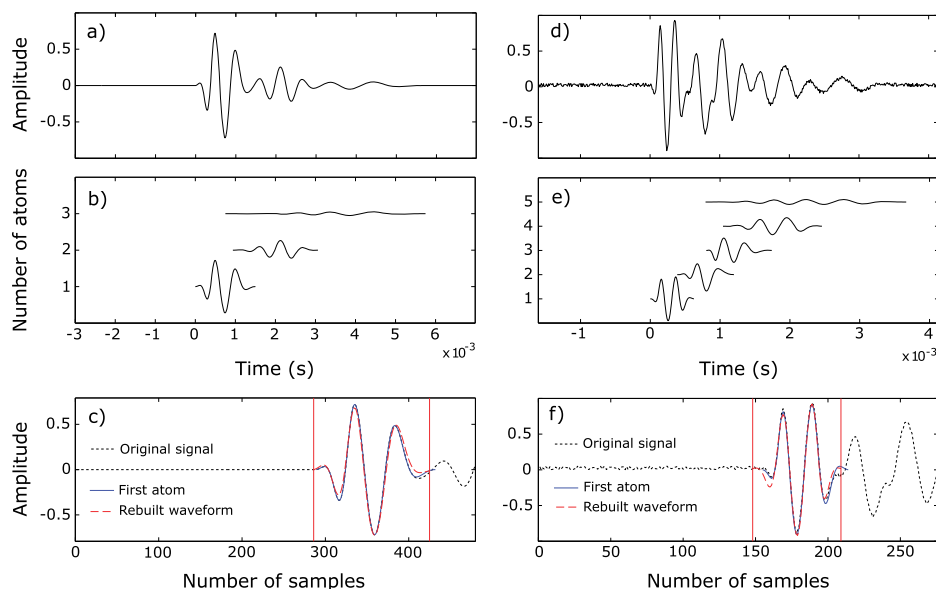


**Figure 3.** Illustration of the processing technique using synthetic signals. (a) Synthetic generated signal of 96 kHz sampling rate constituted by (b) three different summed and overlapped chirp atoms characterized by different amplitude, central frequency and frequency modulation. (c) Our algorithm scans the beginning of the coherent signal to find the best chirp atom (i.e. best correlation). Original signal and first atom are the dotted black line and the solid blue line, respectively, and the dashed red line corresponds to the rebuilt first waveform. (d) Second example of synthetic signal with 5% additive noise constituted by (e) five different summed and overlapped chirp atoms, (f) first arrival reconstruction. This technique is able to correctly rebuild the waveform of the first arrival and then to retrieve its amplitude and frequency components. For both examples presented here, the confidence of the reconstruction procedure (recovered energy of the rebuilt waveform) is over 97% of the selected signal portion indicated by the vertical solid red lines. This figure is available in colour online at [wileyonlinelibrary.com/journal/espl](http://wileyonlinelibrary.com/journal/espl)

rather than detectable impulsive signals. Hence four classes of gravels are considered: class 1 from 2 to 8 mm, class 2 from 8 to 16 mm, class 3 from 16 to 31.5 mm and class 4 from 31.5 to 63 mm. The effect of impact velocity has to be gauged in order to determine the overall impact signature for various flow intensities. By performing two rotating flume experiments, Attal and Lave (2009) observed a linear relationship between the mean fluid velocity and the mean gravel velocity for similar ranges of flow velocities and grain sizes. By varying the slope of the flume from 2° to 10°, we consequently change the flow and gravel velocities as well as the impact velocity by favouring the saltation process as opposed to rolling motion. Using the Manning formula for open rectangular channel to convert the slope information to flow velocity (Chanson, 2004), we define the range of conditions replicated in the experiments for impact measurements in the well-known Hjulström diagram (Figure 4). The grey rectangle in Figure 4 is bounded by grain size and flow velocity limits where the laboratory impact measurements are assumed to be representative of such flow conditions, mostly characterized by transport and erosion processes.

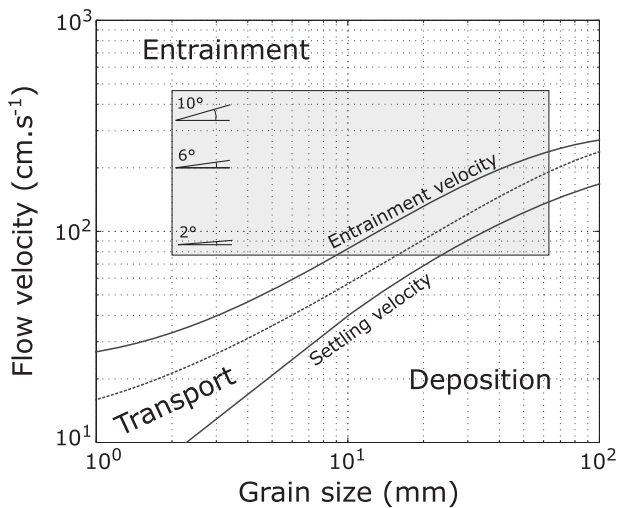


**Figure 4.** Range of conditions replicated in the experiments (grey rectangle) for impact measurements in the Hjulström diagram. The slope corresponding to flow velocity calculated using the Manning formula is also indicated:  $V = n^{-1} R^{2/3} S^{1/2}$ , where  $n$  is the Manning coefficient ( $\approx 0.01$  for PVC with smooth inner walls),  $R$  is the hydraulic radius of the flow cross-section (in metres) and  $S$  corresponds to the slope of the channel bottom (in  $m\ m^{-1}$ ).

One kilogram of each grain class is flushed twice for the three slopes, except for the lowest slope and class 4 because the flow was unable to move the coarsest sediments. This observation confirms the predicted immobility of such coarse materials with the slope set to 2° (lower right corner of the grey rectangle in Figure 4). In Figure 5, the occurrence and the mean confidence of detected impacts are represented in normalized A–F maps. The confidence value, corresponding to the quality of the reconstruction of the first arrival obtained with the FAAD algorithm, is high for most of the retrieved impacts. More than 80% of the total number of rebuilt first arrival waveforms ( $n = 1799$ ) could recover at least 75% of the original signal energy (87% on average). The main information in this figure is the different patterns highlighted on the occurrence maps between the four sediments classes. From class 1 to 4, the impact signature shifts from high frequency–low amplitude to low frequency–high amplitude values. This is clear evidence that the analogy with the Hertz contact theory is relevant. Furthermore, these results indirectly indicate that the effect of impact velocity is sufficiently small in the considered range to observe the predominant effect of grain size. However, there is an overlap between the different frequency and amplitude bands due to the high variability of impact types, grain shapes and impact velocities, which could mask the grain size information in the case of avalanches of mixed grain sizes. Therefore, we test this approach in the following part by analysing the A–F distribution of ‘mixed grain classes’ experiments. For the sake of notation simplicity, the ‘single grain class’ experiments are now referred to as ‘reference experiments’.

‘Mixed grain classes’ experiments

Ten sediment transport experiments are performed with the Trondheim flume. For each experiment, the weight and  $D_{50}$  of materials collected in the basket are estimated. The weight of sampled sediments varies from around 2 to 16 kg, with  $D_{50} = 2–14$  mm and  $D_{90} = 5–35$  mm. Water flow depth is unfortunately unknown but we can fairly assume that flow velocity lies within the same range as for the reference Trier experiments. Motion of very coarse grains ( $>30$  mm) was restricted due to the low slope. Therefore, we used once again the Trier flume in order to record avalanches of grains with large  $D_{50}$ . Two to three repeated flush experiments of sieved materials with identical median grain size were performed using the largest slope (10°). Four different  $D_{50}$  (around 18 to 35 mm) were

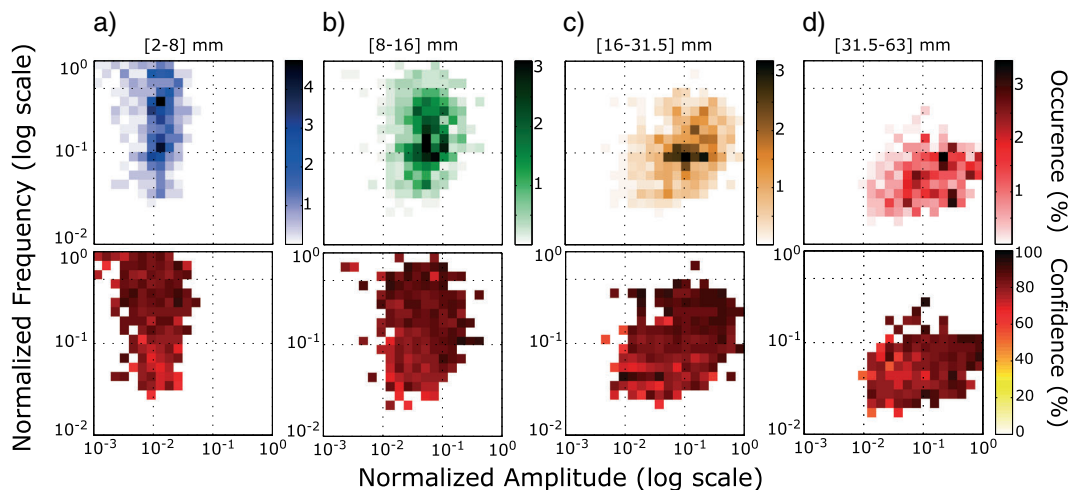


**Figure 5.** Occurrence and mean confidence of detected impacts analysed with the FAAD processing and represented in normalized A–F map for (a) class 1, (b) class 2, (c) class 3, and (d) class 4. For all plots, A–F attributes are normalized by the same maximum amplitude (class 4) and frequency (class 1) values. This figure is available in colour online at [wileyonlinelibrary.com/journal/espl](http://wileyonlinelibrary.com/journal/espl)

investigated. The information relative to these two flume experiments is provided in Table I.

Figure 6 shows the results extracted from the analysis of the aforementioned experiments using the FAAD procedure. For comparison with the reference experiments, frequency and amplitude positions of each recorded impact processed in the reference records are depicted as small markers with dull colours and rectangles corresponding to the 10th to the 90th percentiles boundaries. It is interesting to note that the median *A–F* signatures for experiments with sediment mixtures corresponding to small  $D_{50}$  and consequently composed to a large proportion of small grains (<8 mm) have a similar position in the *A–F* map as class 1 impacts in the reference experiments (blue rectangle). A shift toward class 4 impacts (red rectangle) is observed for experiments with large  $D_{50}$  and containing a smaller proportion of small grains. Therefore a statistical analysis (median) of ‘mixed grain classes’ impact recordings in the *A–F* map allows for a correct retrieval of the median grain size of the sediments moving over the plate for  $D_{50}$  values ranging from 2 to 35 mm.

The following observations also support the robustness of our approach:

- For the Trondheim experiments, notable proportions (6–19%) of sediments smaller than 2 mm were also collected in the basket. This implies that the *A–F* median is a reliable proxy of the median grain size even if sand fraction constitutes a significant part of the bedload transport.
- The average sediment transport rate (i.e. total weight of transported sediments per metre and per total time of impact signal recording) is significantly different between each single experiment, notably between Trier and Trondheim (Table I). However, the statistical approach leading to the estimate of the median value is insensitive to this highly variable parameter.

- The results presented in Figure 6 are the combination of three different experiments using two different set-ups and channel properties. This appears to confirm that the *A–F* signatures are only dependent on the plate set-up. Therefore, we establish in the next part a calibration relationship between *A–F* attributes and  $D_{50}$  to be applied to impact measurements during a flood event in the Olewiger gravel-bed stream.

### Calibration curve between $D_{50}$ and acoustic attributes

In view of the results obtained so far, it seems relevant to look for a calibration curve between  $D_{50}$  and the acoustic attributes because grain size has a clear effect on amplitude (which increases with increasing grain size) and frequency (which decreases with increasing grain size) (Figures 5 and 6). In light of these observations, we propose deriving a general power law relation such as:

$$\log(D_{50}) = C_1 \log[\text{median}(A^a/F^b)] + C_2,$$

where  $a$  and  $b$  are real exponents. As discussed previously, the experimental relationship between  $D_{50}$  and acoustic attributes is constrained by specific ranges of flow velocity and grain size (Figure 4). Hence, this calibration model is built under the reasonable assumption that variations of impact velocity are weak enough to avoid any substantial deviations from this linear dependency. For the sake of notation simplicity, the median calculation for all reference and ‘mixed grain classes’ experiments is implicit in the following analysis. We perform a grid-search calculation of best fitting curves (in the least-square sense) for any  $a–b$  satisfying this relation with a fixed value of slope  $C_1$ . Note that it is always possible with the above relation to find another couple  $a–b$  that leads to a

**Table I.** Main characteristics (slope, discharge,  $D_{50}$ , weight and mean transport rate) of the ‘mixed grain classes’ experiments

Flume	Trondheim										Trier			
Slope	2°										10°			
Discharge (l s <sup>-1</sup> )	47	53	61	68	69	63	59	70	75	69	<5			
$D_{50}$ (mm)	2.4	2.5	2.2	3.4	2.5	3.4	2.7	13.8	3.4	8.3	22	27	35	17.8
Weight (kg)	5.9	15.8	5.1	10.8	3.3	1.9	4.2	2.7	2.1	2.2	8	9	6	4
Transport rate (g m <sup>-1</sup> s <sup>-1</sup> )	25	28	16	26	8	9	6	10	6	3	732	481	347	486

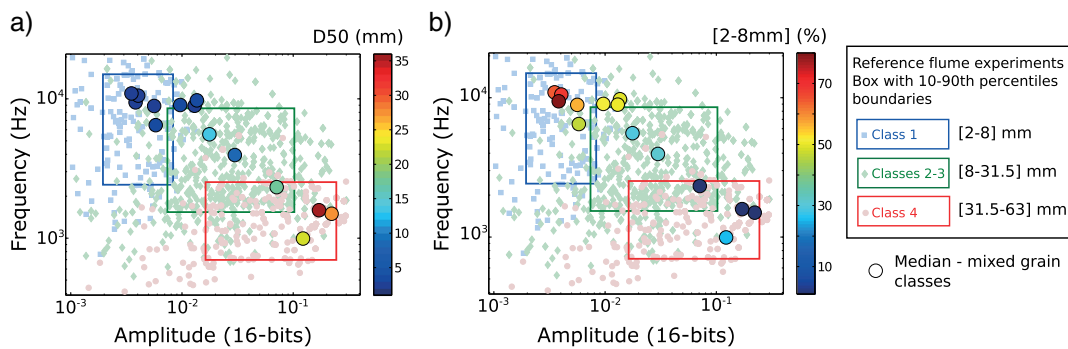


**Figure 6.** The *A–F* signatures for reference (‘single-grain classes’) and ‘mixed grain classes’ experiments (Table I). For the reference experiments, rectangles and small markers with dull colours correspond to class 1 (blue box and square marker), class 2 + 3 (green box and diamond marker) and class 4 (red box and round marker). Classes 2 and 3 are combined into one single intermediate class (8–31.5 mm) for a better visualization. The three rectangles correspond to the 10th and 90th percentiles boundaries of the statistical distributions in the *A–F* map for the reference grain classes. The bigger round markers represent the median values of *A–F* attributes filled with a colour dependent on (a) the value of  $D_{50}$  and (b) proportion of class 1 grains. (See online version for the references to colour in this figure). This figure is available in colour online at [wileyonlinelibrary.com/journal/espl](http://wileyonlinelibrary.com/journal/espl)

different slope of the regression line in log-log space, but has the same quality of fit; for this reason, we need to fix one of the three unknowns  $a$ ,  $b$  and  $C_1$ , and we thus search for the optimal couple  $a$ - $b$  leading to a slope equal to unity in the relation. Figure 7a summarizes this procedure where the standard coefficient of determination  $R^2$  is used as quality index. The highest  $R^2$  value ( $=0.949$ ) is obtained for  $a \approx 0.45b$  for any slope value, thus conveying the inter-correlation between the two variables  $A$  and  $F$  (see also Figures 5 and 6). Therefore, we choose this best couple  $a$ - $b$  leading to  $C_1 = 1$  for the following final calibration curve (Figure 7b):

$$D_{50} = 5.0595 \cdot 10^4 A^{0.39} / F^{0.86},$$

Errors bars in Figure 7b correspond to the first and third quartiles of the  $A$ - $F$  ratio. The largest error bars obtained for the Trondheim experiment can be explained by the use of a wider plate, hence a larger variability of impact location. However, as stated earlier, the median calculation for each experiment appears to be a robust statistical parameter, allowing a reliable regression line to be defined throughout the range  $D_{50} = [1-70]$  mm. Note as well that the complementarity between the different experiments is quite remarkable.

Defining a fair uncertainty is a key point for further quantitative purposes. Our dataset is well scattered along a wide  $D_{50}$  range but the total of 18 measurements might be considered rather small to establish classical confidence intervals. Hence, we compute the 95% prediction interval taking also into account the standard deviation of a future observation, which leads to additional uncertainty. This predictive error, always wider than the standard confidence interval, is a suitable property to develop a calibration model. It allows defining a range of  $D_{50}$  values for which we expect that, for a given  $A$ - $F$  ratio, the next estimated  $D_{50}$  lies within this interval with 95% probability. The total error of  $D_{50}$  derived from this prediction interval has a parabolic shape, well approximated by a second-order polynomial equation expressed in Figure 7b. These errors are, not surprisingly, substantial ( $\pm 60\%$ ) given the observed scattering of individual  $A$ - $F$  pair estimates. This implies that estimations of large  $D_{50}$  will be less certain than estimations of small ones, but the essential information of sharp variations in transported grain size can be well detected.

## Flood event in a small gravel-bed river

In a final step, we apply this relationship to recorded impacts during a summer flood event (20 June 2013) in the Olewiger brook. The final results are presented in Figure 8. This typical flash flood event is characterized by a sudden strong increase from 200 to 380 minutes after the onset of the flood event, followed by a longer falling limb of duration 450 minutes and a second weaker event (Figure 8a). Estimated  $D_{50}$  is represented with corresponding uncertainties for each five minutes interval (identical to the sampling rate of water level). The median is calculated when at least 50 impacts are detected to ensure a proper statistical calculation. The variations of  $D_{50}$  are well correlated with the hydrograph and show significant increases of median grain size when the water level exceeds a certain threshold. Strong increases of  $D_{50}$  are notably observed for the first peak flow at 200 minutes, for the second one at 360 to 380 minutes, and to a lesser extent for the peak flow between 1000 and 1200 minutes. Estimated  $D_{50}$  during peak flows are in agreement with the grain size distribution of the surface bed materials and likely correspond to the surface  $D_{50}$  ( $8.7 \pm 3.9$  mm) during peak flow conditions. During base flow conditions, transport does not occur or is characterized by low  $D_{50}$  corresponding to the transport of very small grains ( $< 1$  mm) not considered in our calibration. Figure 8c shows the number of peaks (counts) per minute above the minimum threshold amplitude used in the FAAD algorithm. This value does not correspond to the number of impacts used in the FAAD processing because many counts can be part of the same impact. Since the mean  $D_{50}$  of bedload transport and instant number of counts generally increase as a function of water discharge, the trend of both shows some similarity (Figures 8b and 8c). However, we failed to obtain a relationship between these two variables for the laboratory experiments, which means a calibration could not be established for peaks counting with the grain size distribution. Nonetheless, the number of counts as displayed in Figure 8c provides qualitative information about the instantaneous transport rate and could be useful to constrain the temporal dynamic of bedload transport in addition to the estimated grain size.

## Discussion

In the framework of acoustic analysis of marine sediment transport, several studies already highlighted the inverse

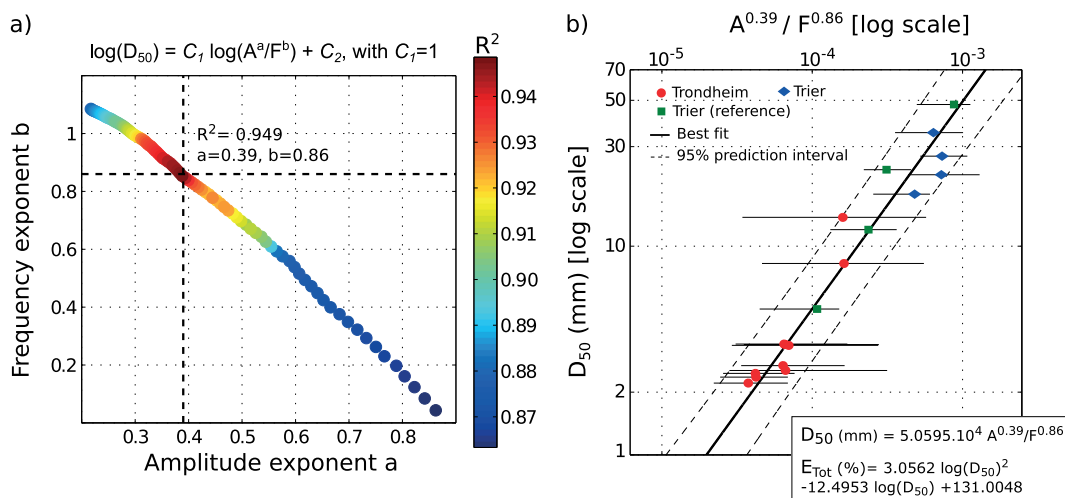


**Figure 7.** (a)  $R^2$  (colour scale) of  $\log(D_{50}) = C_1 \log[\text{median}(A^a/F^b)] + C_2$ , as a function of the amplitude and frequency exponents for  $C_1 = 1$ , (b) final calibration curve (solid black line) between the median grain size ( $D_{50}$ ) and  $A^{0.39}/F^{0.86}$ . The 95% prediction intervals are represented by the dashed black lines and the corresponding total error  $E_{\text{Tot}}$  for  $D_{50}$  is expressed in the inset. (See online version for the references to colour in this figure). This figure is available in colour online at [wileyonlinelibrary.com/journal/espl](http://wileyonlinelibrary.com/journal/espl)

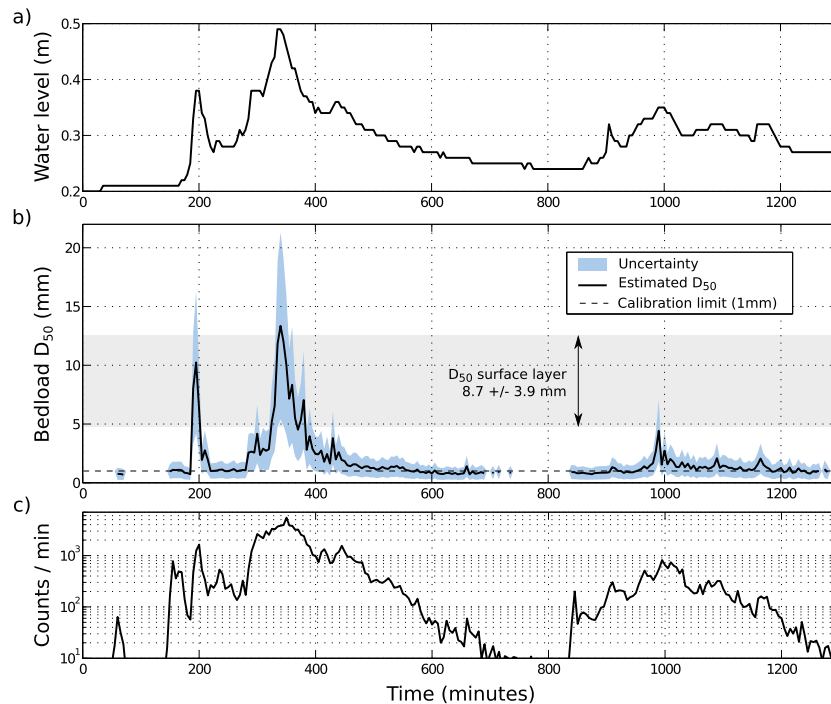


**Figure 8.** Flash flood event (20 June 2013) in the Olewiger brook. (a) Hydrograph, (b) estimated  $D_{50}$  using the power law relation in Figure 7b with associated uncertainties (blue area) and the range of riverbed surface  $D_{50}$  (grey rectangle), (c) temporal variations of peaks counting. (See online version for the references to colour in this figure). This figure is available in colour online at [wileyonlinelibrary.com/journal/espl](http://wileyonlinelibrary.com/journal/espl)

relationship between frequency and grain size (Thorne, 1985, 1990; Bassett *et al.*, 2013). Using a hydrophone scanning the sonic to ultrasonic band mounted in a rotating drum, Thorne (1985) observed significant variations of mean peak frequencies from approximately 10 to 100 kHz for uniformly sized particle mixtures of diameter 0.9 to 12 mm and determined the predominant acoustic source as inter-particle collision. Thorne (1990) performed similar measurements in a marine environment with gravel transport and noticed a good agreement between the shape of ambient noise spectra between laboratory and field observations. Using a hydrophone located in a tidal channel, Bassett *et al.* (2013) observed a relationship between the particle sizes (gravels to pebbles, around 4 to 170 mm) and peak noise levels at lower frequencies from 4 to 20 kHz, corresponding approximately to our measurement frequency range. However, the relationship between characteristic frequencies and particles sizes between these studies and the present one (frequency ranging from around 0.5 to 11 kHz, grain size from 1 to 63 mm) are quite different, most probably due to the nature of the source, the medium of wave propagation and the sensor configuration.

Recently, progress has also been made in the characterization of the material regarding the size of bedload particles, using the Swiss plate geophone (Rickenmann *et al.*, 2014). In this preliminary attempt of extracting grain size information, a promising relationship is obtained between the maximum signal amplitude and the mean  $b$ -axes of the transported particles larger than 10 mm. However, the authors noticed that this relationship is not well constrained, with a large scattering of the dataset and the need of some amplitude correction, whereas our approach appears to be equally applicable to different places because it only depends on the plate/sensor configuration and is sensitive to smaller particles (above 1 mm). In addition, it is probably nearly independent of the test site for a typical range of flow velocities in gravel-bed rivers (approximately  $0.8$  to  $5$  m s<sup>-1</sup>). The estimated  $D_{50}$  using  $A-F$  ratio analysis is thus a critical improvement in the characterization of the time-varying properties of bedload transport with

impact plate systems. Nonetheless, no comparison with collected sediments in the field is hitherto available but the presented results strongly support the reliability of such laboratory calibration and further promising applications in gravel-bed rivers. A new field site in a similar gravel-bed stream (Koulbich River, Colpach, Luxembourg) is already equipped with the same plate set-up placed directly in front of a bedload collector on the streambed. The principal aim of this new field experiment will be to apply and test the processing approach developed in this article at another field site. For a complete bedload transport analysis, the calibration of peak counting with collected sediments, as done with the Swiss plate geophone, is planned for the total bedload flux estimation of each single flood event. Indeed, the number of counts (Figure 8c) must be associated with the number of impulses estimated with the Swiss plate geophone (Rickenmann *et al.*, 2012, 2014). As already studied by Rickenmann *et al.* (2014), the number of impulses is the most accurate variable related to the total transported mass, but a large range of mass values is needed to get a reliable relationship. According to these studies, it is possible to estimate the total bedload flux more accurately after a single flood event than monitoring continuously the amount of transported material. For the well-studied Erlenbach stream, the best fit is obtained using bedload mass data over three-orders of magnitude. Moreover, the scattering of impact data is more important for low mass values. This observation was also noticed in our flume experiments where no significant relationship was found between the total mass recovered in the basket sampler and the total number of impulses. Therefore, collecting sediments in the field after several flood events appears to be the best option to complete this laboratory dataset.

From a practical point of view, the configuration of the plate set-up and the intrinsic properties of the sensor are of primary importance to ensure the reproducibility of this analysis in different places around the world. Indeed, a proper recording of the plate wave mode generated by the grain impact requires the installation of the sensor directly on the contact plate.

Moreover, the sensor should have a wide-band and stable frequency response in the sonic frequency range to correctly retrieve the signature of each single impact with the FAAD procedure. The sensor used in this study has the suitable properties, since it was designed for shallow water applications and is, therefore, perfectly waterproof. However, cheaper sensors such as the piezoelectric accelerometer could be used if waterproof conditions can be guaranteed.

## Conclusion

Results from laboratory flume experiments and one single summer flood event in a gravel-bed stream show that large and small gravel material is well identified by the corresponding frequency and amplitude attributes. The FAAD algorithm used to extract such properties from impact measurements is very promising in view of estimating the temporal variability of median grain size and quantifying processes of bedload transport in rivers. To our knowledge, this is the first time that such an essential bedload property is estimated with high temporal resolution (minutes range) using an impact plate system, confirming the potential of this kind of bedload surrogate monitoring technique in accordance with recent developments in this research domain (Rickenmann *et al.*, 2013). In order to fully exploit the potential of such measurements method, further applications should consider the installation of many identical plates to study the variability of bedload transport along river cross-sections and profiles. This signal decomposition method is also a key to an effective sparse representation of the recorded signal, allowing for the reconstruction of impact signals using the set of seven chirplet parameters characterizing each impact. This method is, therefore, useful to elaborate long-term continuous monitoring preserving the main information of the records and requiring minimal storage capacity.

*Acknowledgements*—This study was supported by the National Research Fund, Luxembourg (BEDLOAD C11/SR/1158445) and could not have been conducted without the help of Jean-Frank Wagner (Department of Geology, Trier University), Wolfgang Feller, Friedrich Weber (both construction of the data logger), and Jochen Aberle (Department of Hydraulic and Environmental Engineering, Norwegian University of Science and Technology, Trondheim) to whom the authors would like to express their gratitude. The authors also thank Mikael Attal, an anonymous reviewer and the Associate Editor for their comments which helped improving the original manuscript.

## References

- Adrian PS. 2002. *The Illustrated Wavelet Transform Handbook*. Institute of Physics Publishing: Bristol.
- Attal M, Lave J. 2009. Pebble abrasion during fluvial transport: experimental results and implications for the evolution of the sediment load along rivers. *Journal of Geophysical Research* **114**: 1–22. DOI: 10.1029/2009JF001328
- Badoux A, Andres N, Turowski JM. 2014. Damage costs due to bedload transport processes in Switzerland. *Natural Hazards and Earth System Sciences* **14**: 279–294. DOI: 10.5194/nhess-14-279-2014
- Bardainne T, Gaillot P, Dubos-Sallée N, Blanco J, Sénéchal G. 2006. Characterization of seismic waveforms and classification of seismic events using chirplet atomic decomposition. Example from the Lacq gas field (Western Pyrenees, France). *Geophysical Journal International* **166**(2): 699–718. DOI: 10.1111/j.1365-246X.2006.03023.x
- Barton JS, Slingerland RL, Pittman S, Gabrielson TB. 2010. Monitoring coarse bedload transport with passive acoustic instrumentation: a field study. In *Bedload-surrogate Monitoring Technologies*, Gray JR, Laronne JB, Marr JDG (eds), US Geological Survey Scientific Investigations Report SIR 2010-5091. US Geological Survey: Reston, VA.
- Bassett C, Thomson J, Polagye B. 2013. Sediment-generated noise and bed stress in a tidal channel. *Journal of Geophysical Research – Oceans* **118**: 2249–2265. DOI: 10.1002/jgrc.20169
- Belleudy P, Valette A, Graff B. 2010. Passive hydrophone monitoring of bedload in river beds: first trials of signal spectral analyses. In *Bedload-surrogate Monitoring Technologies*, Gray JR, Laronne JB, Marr JDG (eds), US Geological Survey Scientific Investigations Report SIR 2010-5091. US Geological Survey: Reston, VA.
- Bogen J, Fergus T, Walling DE (eds). 2003. *Erosion and Sediment Transport Measurement in Rivers, Technological and Methodological Advances*. International Association of Hydrological Sciences (IAHS) Publication: Wallingford.
- Burtin A, Hovius N, McArdeell BW, Turowski JM, Vergne J. 2014. Seismic constraints on dynamic links between geomorphic processes and routing of sediment in a steep mountain catchment. *Earth Surface Dynamics* **2**: 21–33. DOI: 10.5194/esurf-2-21-2014
- Buttle DJ, Scruby CB. 1990. Characterization of particle impact by quantitative acoustic emission. *Wear* **137**: 63–90. DOI: 10.1016/0043-1648(90)90018-6
- Chanson B. 2004. *Hydraulics of Open Channel Flow*. Elsevier Butterworth Heinemann: Oxford.
- Coppens F. 1985. First arrival picking on common-offset trace collections for automatic estimation of static corrections. *Geophysical Prospecting* **33**: 1212–1231. DOI: 10.1111/j.1365-2478.1985.tb01360.x
- Earle PS, Shearer PM. 1994. Characterization of global seismograms using an automatic-picking algorithm. *Bulletin of the Seismological Society of America* **84**: 366–376.
- Ergenzinger P, Schmidt KH. 1993. *Dynamics and Geomorphology of Mountain Rivers*. Springer Verlag: Berlin.
- Gomez B. 2006. The potential rate of bed-load transport. *Proceedings of the National Academy of Sciences* **103**(46): 17170–17173. DOI: 10.1073/pnas.0608487103
- Goupillaud P, Grossman A, Morlet J. 1984. Cycle-octave and related transforms in seismic signal analysis. *Geoexploration* **23**: 85–102. DOI: 10.1016/0016-7142(84)90025-5
- Gray JR, Laronne JB, Marr JDG. 2010. *Bedload-surrogate Monitoring Technologies*. US Geological Survey Scientific Investigations Report SIR 2010-5091. US Geological Survey: Reston, VA.
- Gribonval R. 2001. Fast matching pursuit with a multiscale dictionary of Gaussian chirps. *IEEE Transactions on Signal Processing* **49**(5): 994–1001. DOI: 10.1109/78.917803
- Habersack HM, Laronne JB. 2001. Bedload texture in an alpine gravel bed river. *Water Resources Research* **37**(12): 3359–3370. DOI: 10.1029/2001WR000260
- Hegg C, Rickenmann D. 1998. Short-time relations between runoff and bedload transport in a steep mountain torrent. In *Modelling Soil Erosion, Sediment Transport and Closely Related Processes*, Summer E, Zhang W (eds), Proceedings of the Vienna Symposium IAHS Publication no. 249. IAHS Press: Wallingford; 317–324.
- Johnson KL. 1985. *Contact Mechanics*. Cambridge University Press: Cambridge.
- Krein A, Klinck H, Eiden M, Symader W, Bierl R, Hoffmann L, Pfister L. 2008. Investigating the transport dynamics and the properties of bedload material with a hydro-acoustic measuring system. *Earth Surface Processes and Landforms* **33**: 152–163. DOI: 10.1002/esp.1576
- Krein A, Schorer M. 2000. Road runoff pollution by polycyclic aromatic hydrocarbons and its contribution to river sediments. *Water Research* **34**: 4110–4115. DOI: 10.1016/S0043-1354(00)00156-1
- Laronne JB, Reid I. 1993. Very high rates of bedload sediment transport by ephemeral desert rivers. *Nature* **366**: 148–150. DOI: 10.1038/366148a0
- Lord ML, Germanoski D, Allmendinger NE. 2009. Fluvial geomorphology: monitoring stream systems in response to a changing environment. In *Geological Monitoring: Boulder*, Young R, Norby L (eds). Geological Society of America: Boulder, CO; 69–103.
- Mallat S. 1999. *A wavelet tour of signal processing*. Academic Press: Burlington, MA.
- Mallat S, Zhang Z. 1993. Matching pursuits with time–frequency dictionaries. *IEEE Transactions on Signal Processing* **41**(12): 3397–3415. DOI: 10.1109/78.258082
- Mann S, Haykin S. 1995. The chirplet transform: physical considerations. *IEEE Transactions on Signal Processing* **43**(11): 2745–2761. DOI: 10.1109/78.482123

- Mizuyama T, Laronne JB, Nonaka M, Sawada T, Satofuka Y, Matsuoka M, Yamashita S, Sako Y, Tamaki S, Watari M, Yamaguchi S, Tsuruta K. 2010. Calibration of a passive acoustic bedload monitoring system in Japanese mountain rivers. In *Bedload-surrogate Monitoring Technologies*, Gray JR, Laronne JB, Marr JDG (eds), US Geological Survey Scientific Investigations Report SIR 2010-5091. US Geological Survey: Reston, VA.
- Oppenheim AV, Schafer RW, Buck JR. 1999. *Discrete-time Signal Processing*. Prentice Hall: Englewood Cliffs, NJ.
- Pecorari C. 2013. Characterizing particle flow by acoustic emission. *Journal of Nondestructive Evaluation* **32**: 104–111.
- Perrier V, Philipovitch T, Basdevant C. 1995. Wavelet spectra compared to Fourier spectra. *Journal of Mathematical Physics* **36**: 1506–1519. DOI: 10.1063/1.531340
- Petticrew E, Krein A, Walling D. 2007. Evaluating fine sediment mobilization and storage in a gravel-bed river using controlled reservoir releases. *Hydrological Processes* **21**: 198–210. DOI: 10.1002/hyp.6183
- Reid I, Layman JT, Frostick LE. 1980. The continuous measurement of bedload discharge. *Journal of Hydraulic Research* **18**: 243–249. DOI: 10.1080/00221688009499550
- Rickenmann D, Laronne JB, Turowski JM, Vericat D. (eds). 2013. *International Workshop of Acoustic and Seismic Monitoring of Bedload and Mass Movements – Abstracts*. Swiss Federal Institute for Forest, Snow and Landscape WSL: Birmensdorf.
- Rickenmann D, McArdeall BW. 2007. Continuous measurement of sediment transport in the Erlenbach stream using piezoelectric bedload impact sensors. *Earth Surface Processes and Landforms* **32**: 1362–1378. DOI: 10.1002/esp.1478
- Rickenmann D, Turowski JM, Fritschi B, Klaiber A, Ludwig A. 2012. Bedload transport measurements at the Erlenbach stream with geophones and automated basket samplers. *Earth Surface Processes and Landforms* **37**: 1000–1011. DOI: 10.1002/esp.3225
- Rickenmann D, Turowski JM, Fritschi B, Wyss C, Laronne J, Barzilai R, Reid I, Kreisler A, Aigner J, Seitz H, Habersack H. 2014. Bedload transport measurements with impact plate geophones: comparison of sensor calibration in different gravel-bed streams. *Earth Surface Processes and Landforms* **39**: 928–942. DOI: 10.1002/esp.3499
- Thorne PD. 1985. The measurement of acoustic noise generated by moving artificial sediments. *Journal of the Acoustical Society of America* **78**(3): 1013–1023. DOI: 10.1121/1.393018
- Thorne PD. 1990. Seabed generation of ambient noise. *Journal of the Acoustical Society of America* **87**(1): 149–153. DOI: 10.1121/1.399307
- Torrence C, Compo GP. 1998. A practical guide to wavelet analysis. *Bulletin of the American Meteorological Society* **79**: 61–78.
- Tsunoda T, Sano K, Tsuneoka O, Morioka T. 1986. Acceleration signal characteristics for loose part impact. *Journal of Nuclear Science and Technology* **23**(11): 968–978. DOI: 10.1080/18811248.1986.9735085
- Turowski JM, Badoux A, Rickenmann D. 2011. Start and end of bedload transport in gravel-bed streams. *Geophysical Research Letters* **38**: L04401. DOI: 10.1029/2010GL046558
- Turowski JM, Böckli M, Rickenmann D, Beer AR. 2013. Field measurements of the energy delivered to the channel bed by moving bed load and links to bedrock erosion. *Journal of Geophysical Research – Earth Surfaces* **118**: 2438–2450. DOI: 10.1002/2013JF002765
- Turowski JM, Rickenmann D. 2011. Measuring the statistics of bed-load transport using indirect sensors. *Journal of Hydraulic Engineering* **137**: 116–122. DOI: 10.1061/(ASCE)HY.1943-7900.0000277
- Uher M, Benes P. 2012. Measurement of particle size distribution by the use of acoustic emission method. In *Instrumentation and Measurement Technology Conference (I2MTC)*. IEEE International: Graz; 1194–1198. DOI: 10.1109/I2MTC.2012.6229375
- Yager EM, Kirchner JW, Dietrich WE. 2007. Calculating bed load transport in steep boulder bed channels. *Water Resources Research* **43**: W07418. DOI: 10.1029/2006WR005432